Stable intermediate phase regulation for high-performance and scalable perovskite solar cells

Kai Cai[1,2], Yibin Jiao[1,2], Zhuang Xiong[1,2], Hui Wang[1,2], Jiaxin Weng[1,2], Qian Zhang[1,2], Zhengchang Xia[1,2], Chen Zhang[1,2], Huixiong Deng[1,2], Xingwang Zhang[1,2], Haitao Zhou[1,2]*, Jingbi You[1,2]*

[1]State Key Laboratory of Semiconductor Physics and Chip Technologies, Institute of Semiconductors, Chinese Academy of Sciences, Beijing 100083, P. R. China

[2]Center of Materials Science and Optoelectronics Engineering, University of Chinese Academy of Sciences, Beijing 100049, P. R. China

*Corresponding author: haitaozhou@semi.ac.cn (H. Z.) or jyou@semi.ac.cn (J. Y.)

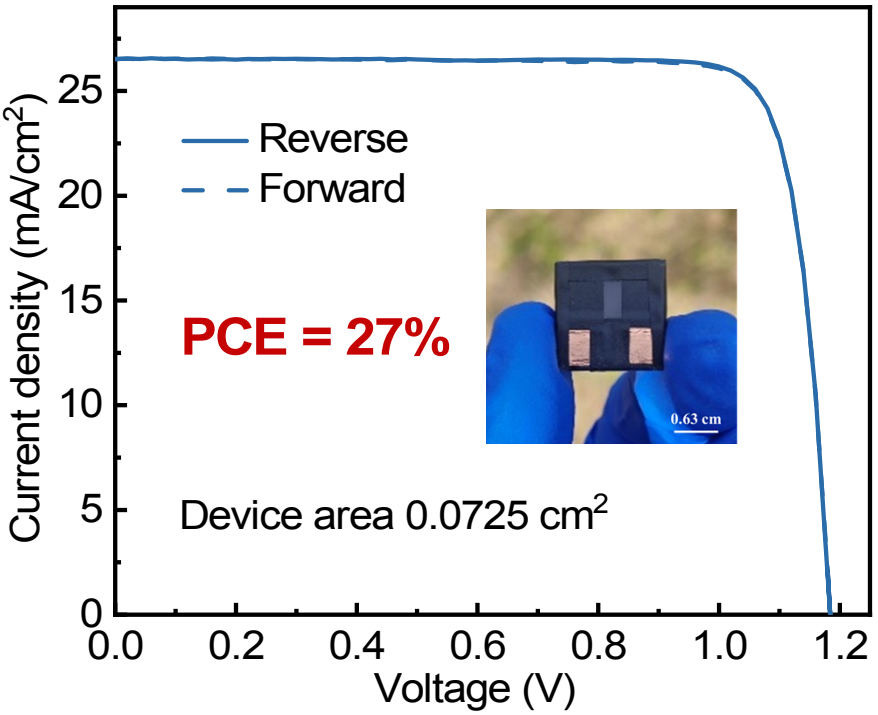

Supplementary Fig. 1 (Color online) Optical photograph and *J-V* curves under forward and reverse scans of small-area perovskite solar cells with a 0.0725 cm^2 device area.

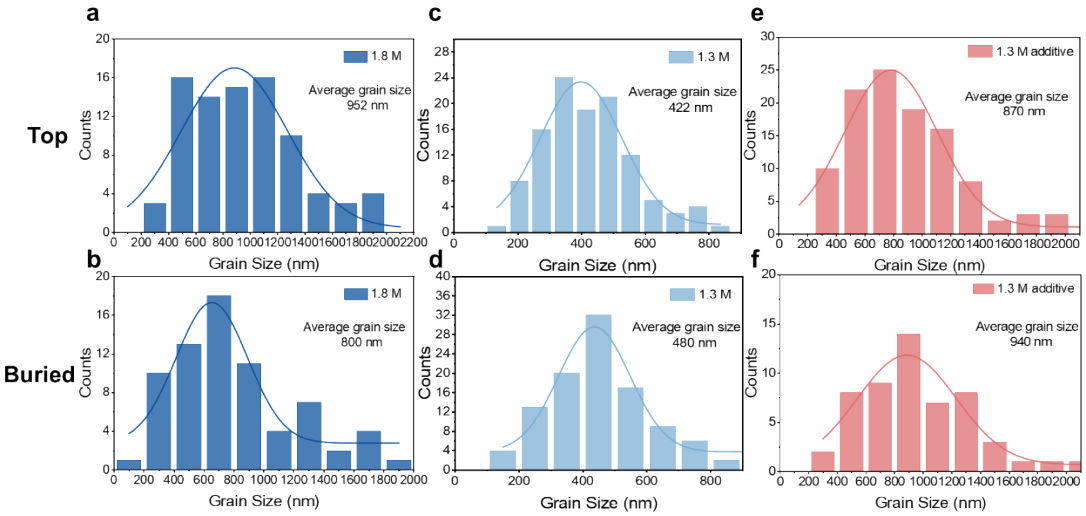

Supplementary Fig. 2 (Color online) Grain size distribution of the top-surface and buried-surface morphologies of perovskite films under different preparation conditions. (a, b) 1.8 M, (c, d) 1.3 M, (e, f) 1.3 M additive.

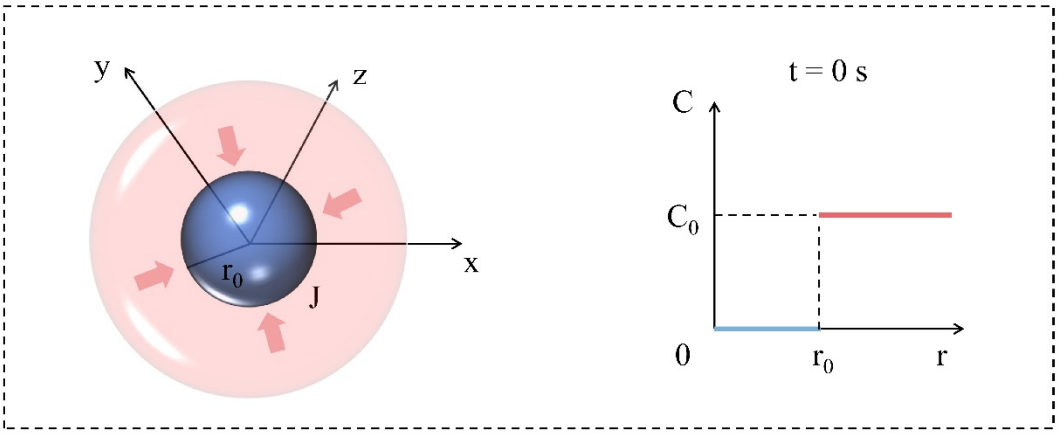

Supplementary Fig. 3 (Color online) Three-dimensional diffusion model. A sphere with radius r_0, where the solute concentration inside the sphere is 0, and the external solute concentration is C_0. The solute diffusion flux into the sphere is *J*. The volume of solid formed by each solute molecule is v.

The concentration changes with time which corresponding to the non-steady state diffusion process. According to the Fick's Second Law of Diffusion.

$$\frac{\partial C}{\partial t} = D\left(\frac{\partial^2 C}{\partial r^2} + \frac{2}{r}\frac{\partial C}{\partial r}\right) \quad (1)$$

Where C is the concentration of diffusing species; □ is the time; □ is diffusion coefficient and r is the radial coordinates.

In order to solve Eq. (1), we set following conditions:

Initial conditions:

$$t = 0, \begin{cases} C_1 = 0, & r < r_0 \\ C_2 = C_0, & r > r_0 \end{cases} \quad (2)$$

Boundary conditions:

$$t \geq 0, \begin{cases} C_1 = 0, & r = 0 \\ C_2 = C_0, & r = +\infty \end{cases} \quad (3)$$

For convenience, we use Boltzmann transform to solve the equation.

We set:

$$u = \frac{r}{2\sqrt{Dt}} \quad (4)$$

Substituting Eq. (4) into Eq. (1),

$$\frac{\partial C}{\partial t} = \frac{\partial C}{\partial u} \cdot \frac{\partial u}{\partial t} = -\frac{r}{4\sqrt{Dt^3}} \frac{\partial C}{\partial u} = D \cdot \left(\frac{1}{4Dt} \frac{\partial^2 C}{\partial u^2} + \frac{1}{r\sqrt{Dt}} \frac{\partial C}{\partial u} \right)$$

Thus Eq. (1) is rewritten as:

$$\frac{\partial^2 C}{\partial u^2} = -2\left(u + \frac{1}{u}\right) \frac{\partial C}{\partial u} \quad (5)$$

We define $\frac{\partial C}{\partial u} = \mu$, then Eq. (5) is rewritten as:

$$\frac{\partial \mu}{\partial u} = -2\left(u + \frac{1}{u}\right) \mu \quad (6)$$

We obtain the solution of Eq. (6):

$$\mu = \frac{A}{u^2} e^{-u^2} \quad (7)$$

Substituting Eq. (7) into $\frac{\partial C}{\partial u} = \mu$, we obtain:

$$\frac{\partial C}{\partial u} = \frac{A}{u^2} e^{-u^2} \quad (8)$$

After integrating, we have:

$$C = -\sqrt{\pi} A \, \mathrm{erf}(u) - \frac{A}{u} e^{-u^2} + B \quad (9)$$

In order for $C(0, t) = 0$, there must be A=0, but this results in $C(r, t) = C_0$, paradox.

Therefore, we need to reconsider the initial conditions.

Since the initial condition is a ladder function, we can directly use the error function solution (The relationship holds when t is sufficiently small).

$$C(r,t) = \frac{C_0}{2}\left(\mathrm{erf}\left(\frac{r - r_0}{2\sqrt{Dt}}\right) + \mathrm{erf}\left(\frac{r + r_0}{2\sqrt{Dt}}\right)\right) \quad (10)$$

Finally, we have diffusive fluxes:

$$J = -4\pi r^2 D \frac{\partial C}{\partial r} = -\frac{2\sqrt{\pi D} r^2 C_0}{\sqrt{t}} \left(e^{-\frac{(r-r_0)^2}{4Dt}} + e^{-\frac{(r+r_0)^2}{4Dt}} \right) \quad (11)$$

the change in particle size with time is given by Eq12

$$\frac{dr}{dt} = \frac{vDC_0}{2\sqrt{\pi Dt}} \left(e^{-\frac{(r-r_0)^2}{4Dt}} + e^{-\frac{(r+r_0)^2}{4Dt}} \right) \quad (12)$$

From Eq. (11), the diffusion flux scales as $J \propto C_0$, indicating that the solute supply is intrinsically limited in low-concentration systems. From Eq. (12), the growth rate satisfies $\frac{dr}{dt} \propto \frac{1}{\sqrt{t}}$.

For $t \to 0$

$$r(t) \approx r_o + 2\sqrt{Dt}\, \mathrm{erf}^{-1}\left(\frac{C_0\sqrt{Dt}}{\sqrt{\pi}}\right)$$

For $t \to \infty$

$$r(t) \approx r_o + 2\mathrm{v}C_0\sqrt{\frac{Dt}{\pi}}$$

This analysis reveals two key factors governing grain growth: the initial concentration determines the flux magnitude, while the growth time dictates the final grain size. Consequently, while low-concentration processing inherently suffers from limited solute flux, prolonging the crystallization window can compensate by allowing more time for grain growth.

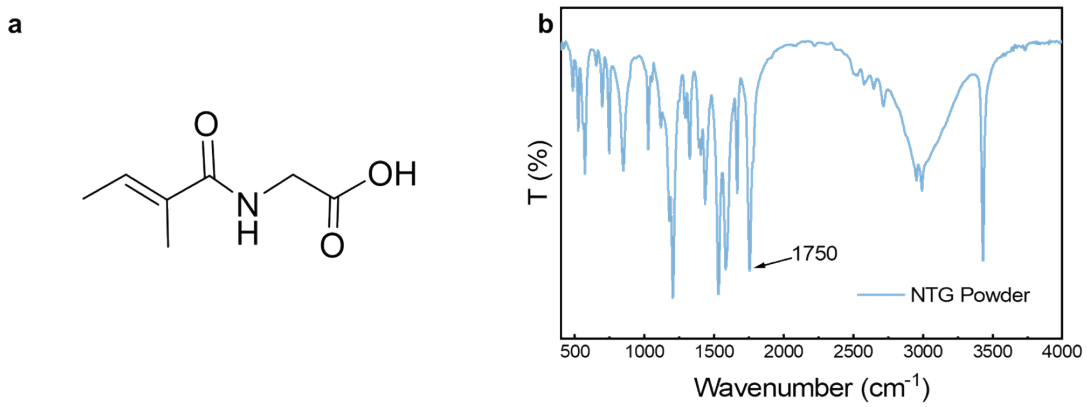

Supplementary Fig. 4 (Color online) (a)Structural formula of NTG ;(b) Fourier transform infrared (FTIR) spectrum of pure NTG powder, which shows the C=O stretching of NTG exists at 1750 cm^{-1}

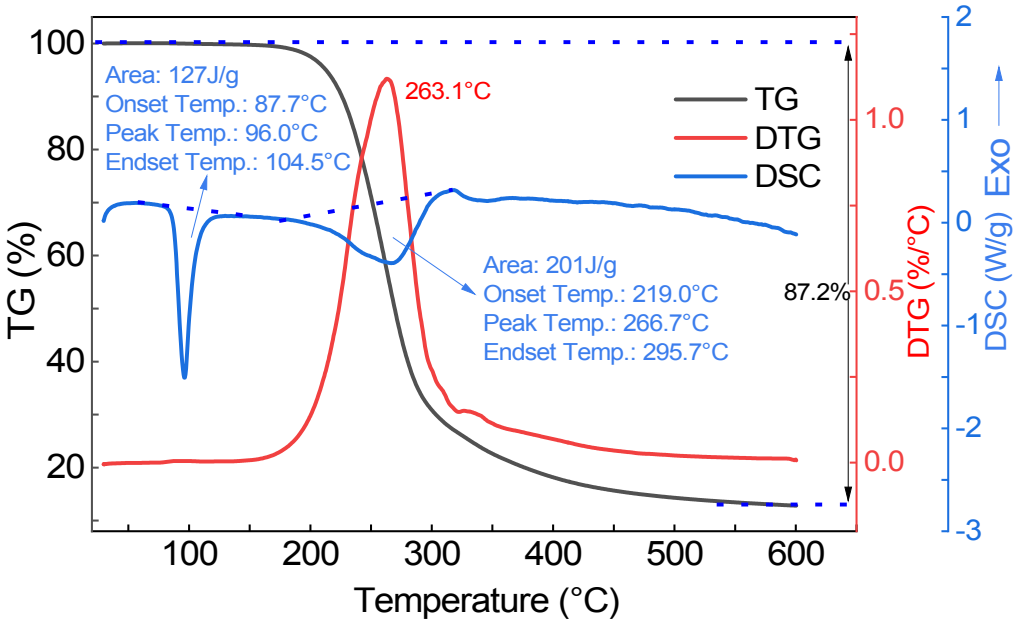

Supplementary Fig. 5 (Color online) Thermogravimetric analysis (TGA) and differential scanning calorimetry (DSC) analysis of NTG powder.

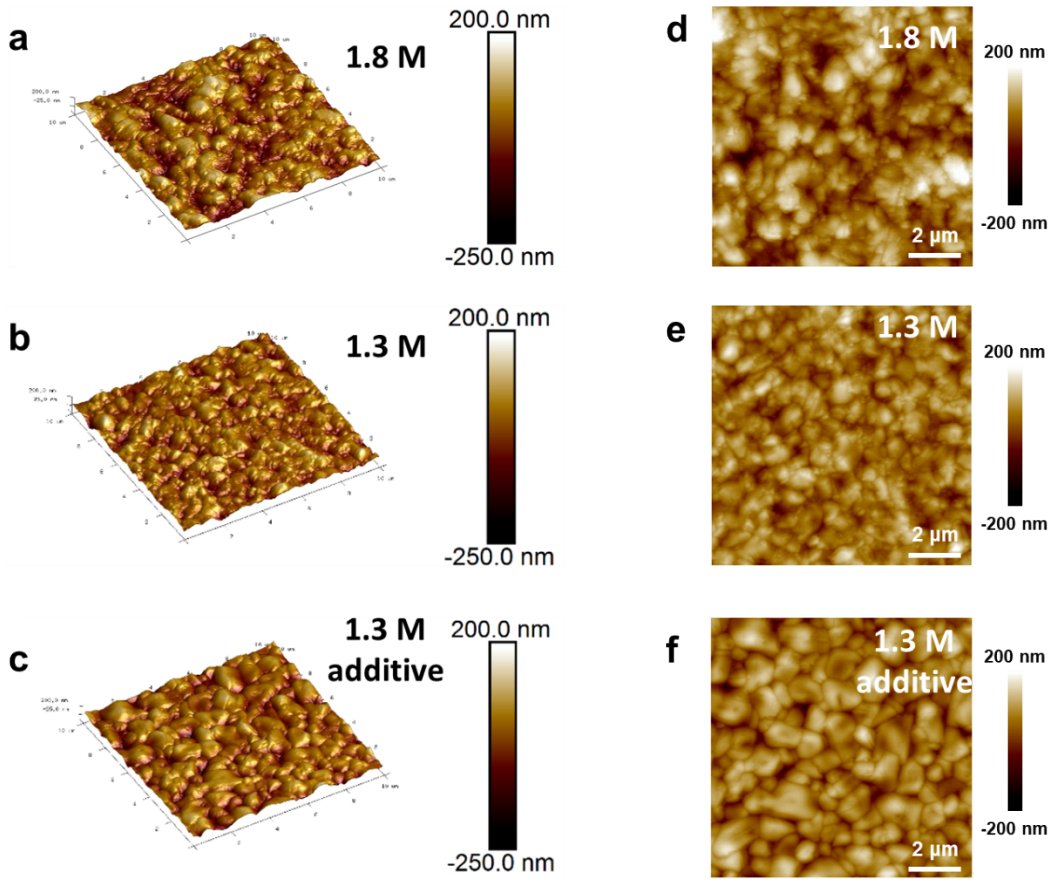

Supplementary Fig. 6 (Color online) 3D and 2D AFM image of perovskite films (a, d)1.8 M; (b, e)1.3 M;(c, f)1.3 M additive

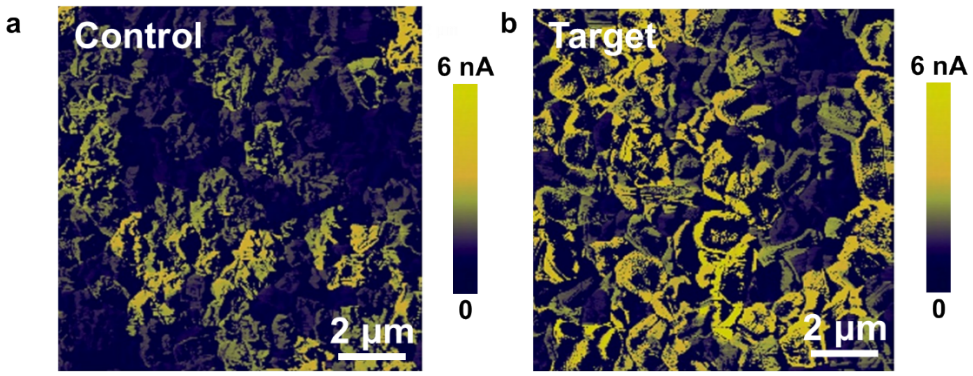

Supplementary Fig. 7 (Color online) C-AFM of perovskite films without (a) and with (b) NTG.

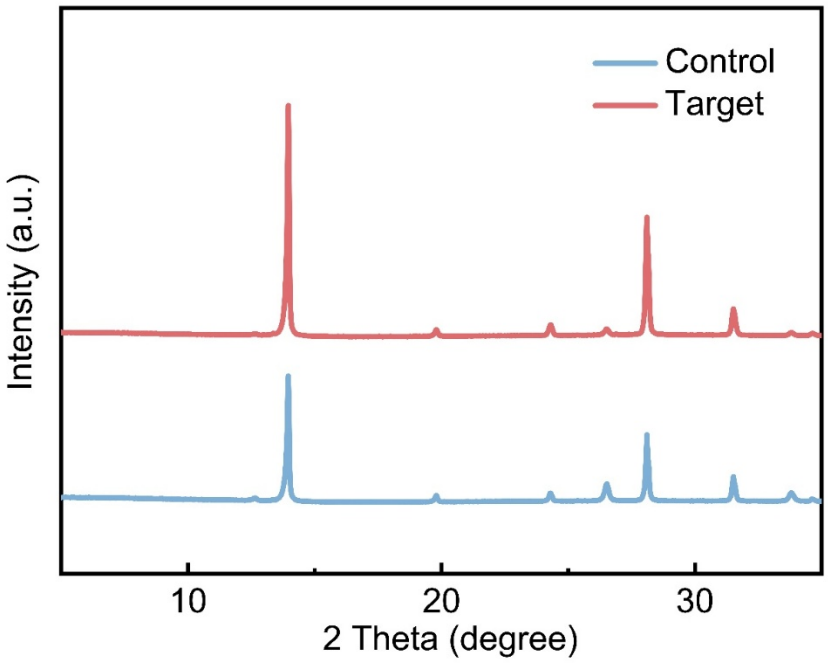

Supplementary Fig. 8 (Color online) XRD spectra of perovskite films without (control) and with (target) NTG.

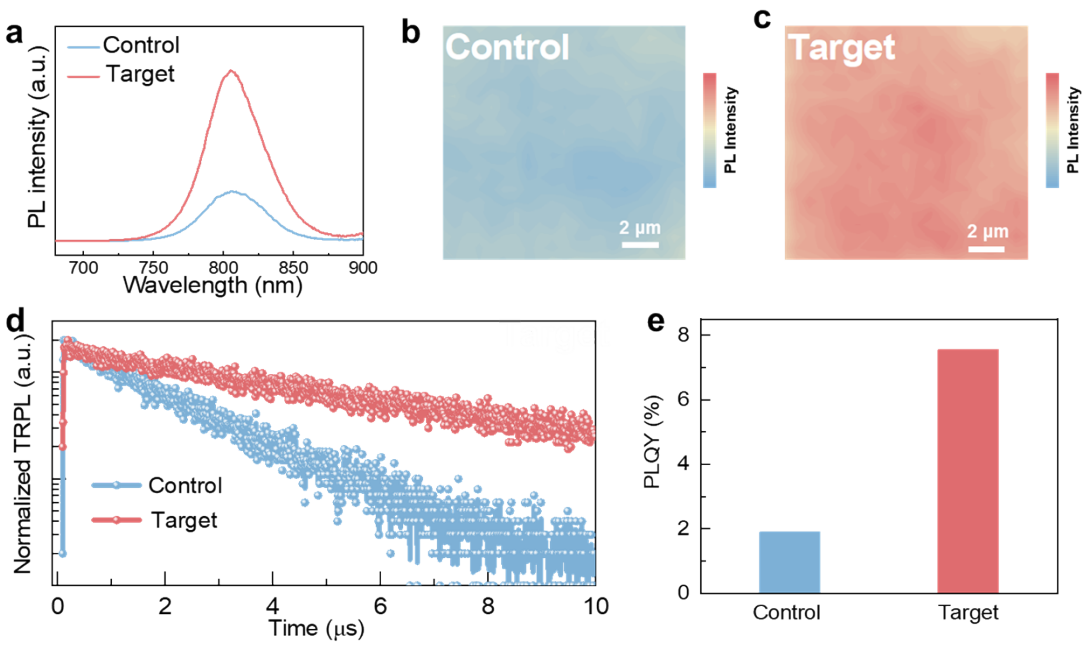

Supplementary Fig. 9 (Color online) (a) Photoluminescence (PL) spectra of perovskite films without (control) and with (target) NTG. (b, c) Photoluminescence (PL) intensity distribution map of perovskite films without (b) and with (c) NTG. (d) Time-resolved photoluminescence (TRPL) spectrum of perovskite films. (e) Photoluminescence quantum yield (PLQY) of perovskite films.

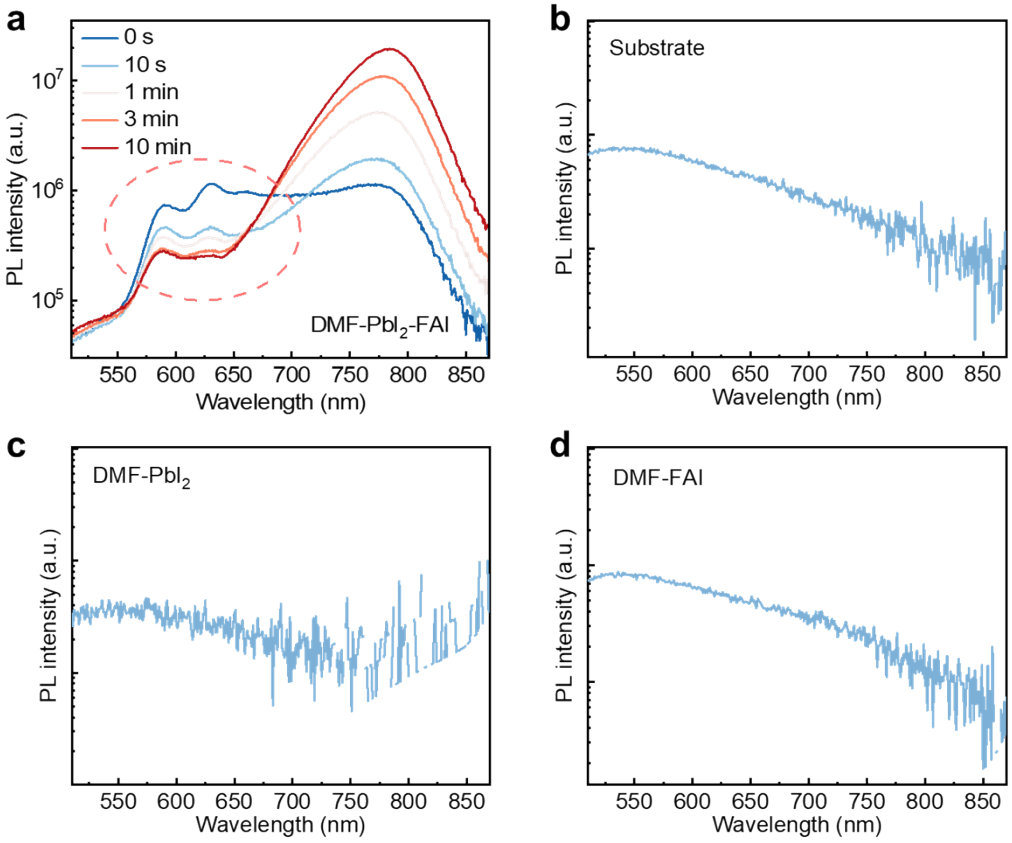

Supplementary Fig. 10 (Color online) PL spectra of samples after vacuum extraction. (a), DMF-PbI_2-FAI annealed in ambient atmosphere for different durations. (b), Substrate (FTO/NiO_x/Me-4PACz). (c), DMF-PbI_2. (d), DMF-FAI.

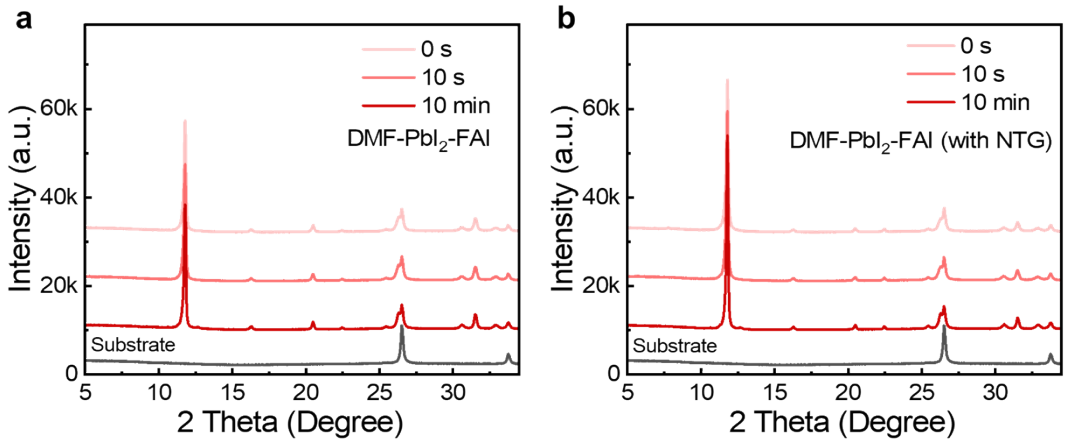

Supplementary Fig. 11 (Color online) XRD spectra of DMF-PbI_2-FAI (a) and DMF-PbI_2-FAI (with NTG) (b) annealed in ambient atmosphere for different durations after vacuum extraction.

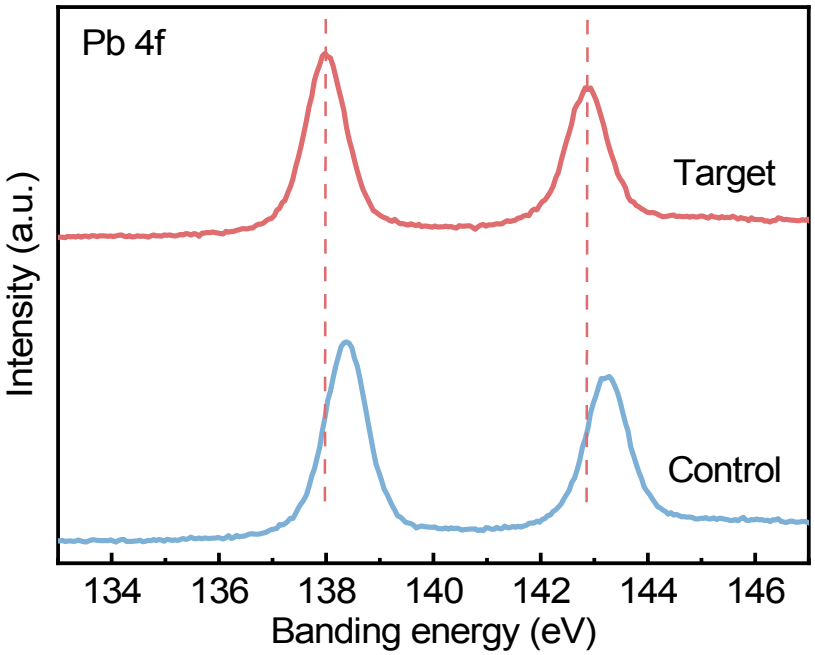

Supplementary Fig. 12 (Color online) XPS spectra of Pb 4f in perovskite films without NTG (control) and with NTG (target).

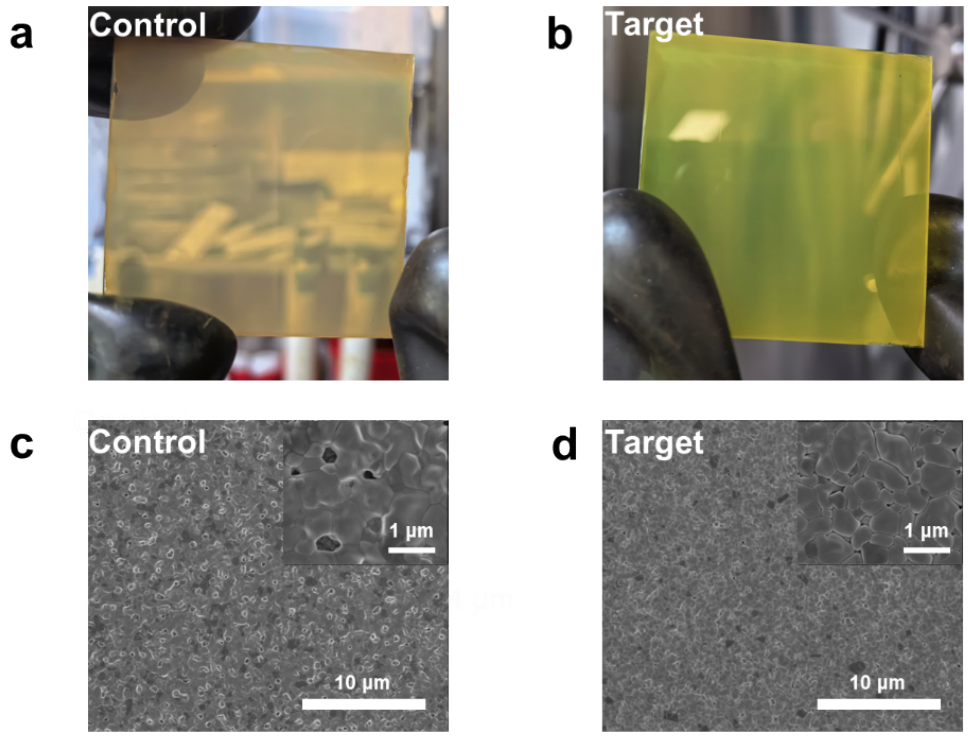

Supplementary Fig. 13 (Color online) Comparison of control (a, c) and target (b, d) perovskite intermediate phase images and SEM

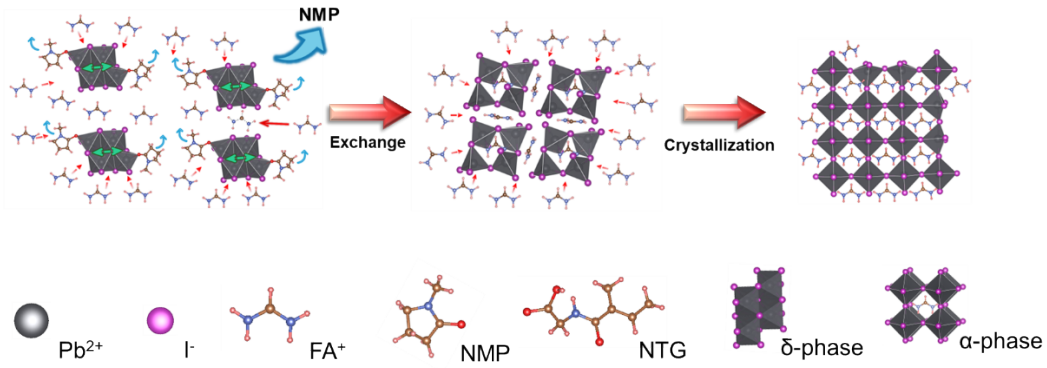

Supplementary Fig. 14 (Color online) The schematic diagram illustrating the crystal structure transformation from the perovskite solution to the final film without additive NTG.

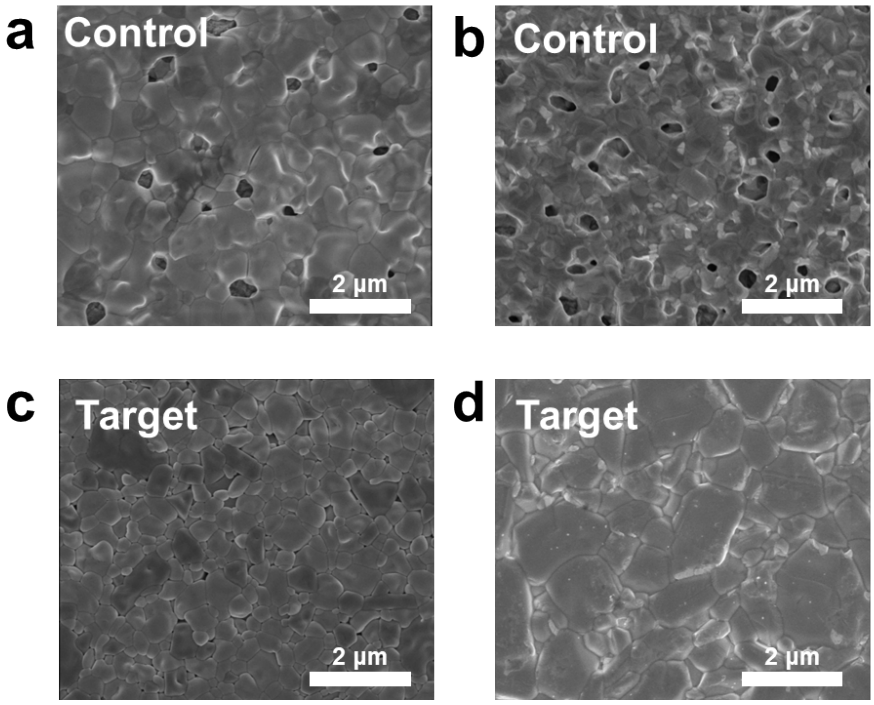

Supplementary Fig. 15 (Color online) SEM images of perovskite intermediate phase films after 24 hours of storage and the corresponding annealed films. (a, b), Control sample: intermediate phase film (a) and annealed film (b). (c, d), Target sample: intermediate phase film (c) and annealed film (d).

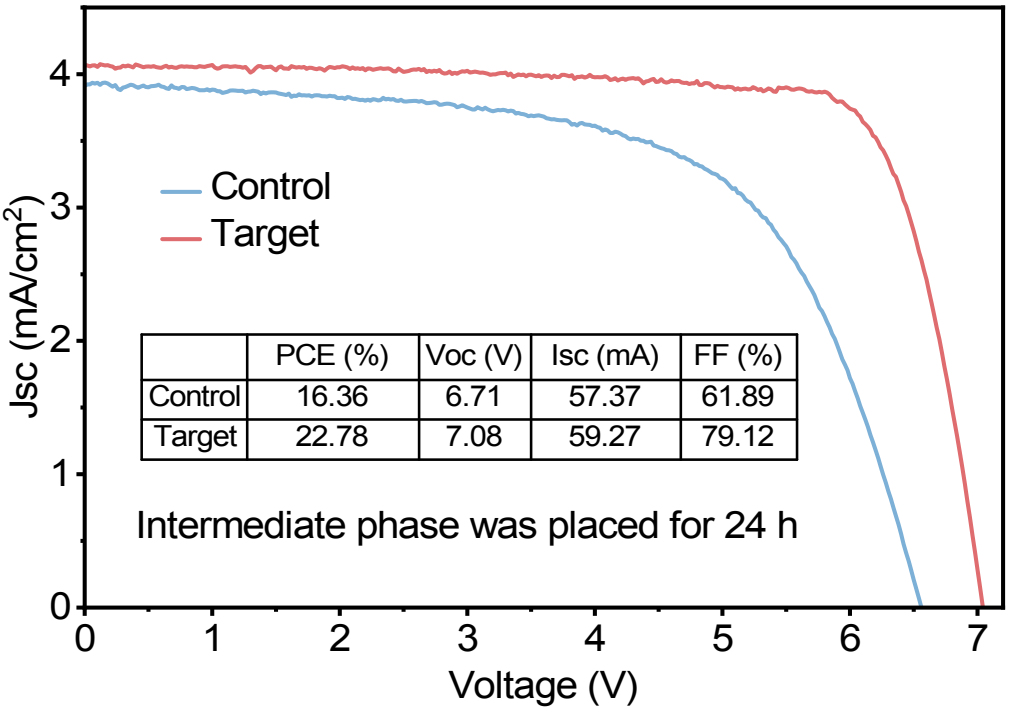

Supplementary Fig. 16 (Color online) Performance comparison of 14.6 cm^2 modules prepared after 24-hour placement of perovskite intermediate phase films of the control and target samples (without MgF_2).

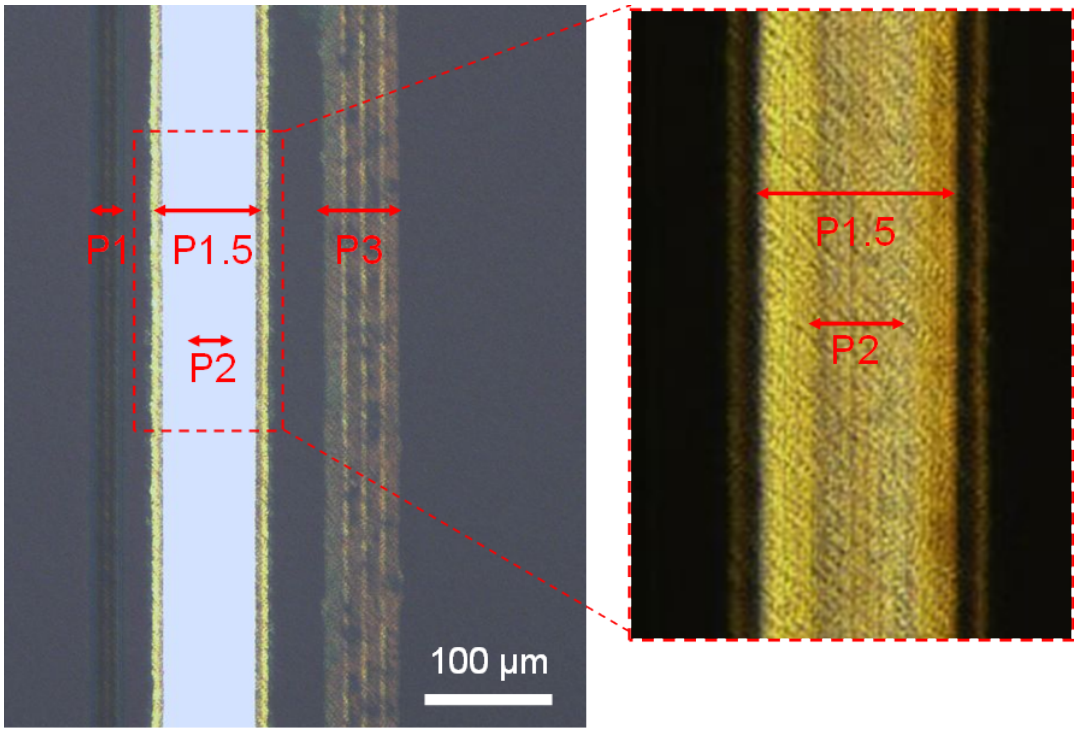

Supplementary Fig. 17 (Color online) Optical microscopy image of the interconnection region between sub-cells in the perovskite module. NTG modification did not alter the laser scribing quality or the geometric fill factor.

Appendix: Summary of the Report
Report No.: GXgf2024-07086
Client: Institute of Semiconductors, CAS
Sample: Perovskite Solar Cell
Type/Model: Perovskite Solar Cell
DUT S/N: 2-M3
Manufacturer: Institute of Semiconductors, CAS
Sample temperature: (25±1)℃
Date of Test: 11/21/2024
Environmental conditions: (22±1) ℃, RH (19±2) %
Mask: An aperture area of 1461.517 mm² (M3#, Certificate No.: CDjc2024-09184)

The test has been conducted by the PV Metrology Lab of NIM (National Institute of Metrology, China). Measurement of irradiance intensity and all other measurements are traceable to the International System of Units (SI). Data in this report apply only at the time of the test for the sample. For more details, please refer to the text of the report.

	Area (mm^2)	I_{sc}(mA)	V_{oc}(V)	P_{max}(mW)
Reverse Scan	1461.517	61.85	7.103	356.0
Forward Scan	1461.517	61.85	7.082	351.8
	I_{max}(mA)	V_{max}(V)	FF (%)	η (%)
Reverse Scan	58.37	6.100	81.04	24.36
Forward Scan	57.67	6.100	80.32	24.07

I-V Characterization Methods:
JJF 1622-2017: Calibration Specification of Solar Cells：Photoelectric Properties
Reference Solar Cell:
Type: Mono-Si
Solar Simulator:
Classification: A+AA+ (Double-light source: Xeon and Halogen);
Total irradiance: 1000 W/m² based on I_{sc} of the above Reference Solar Cell.

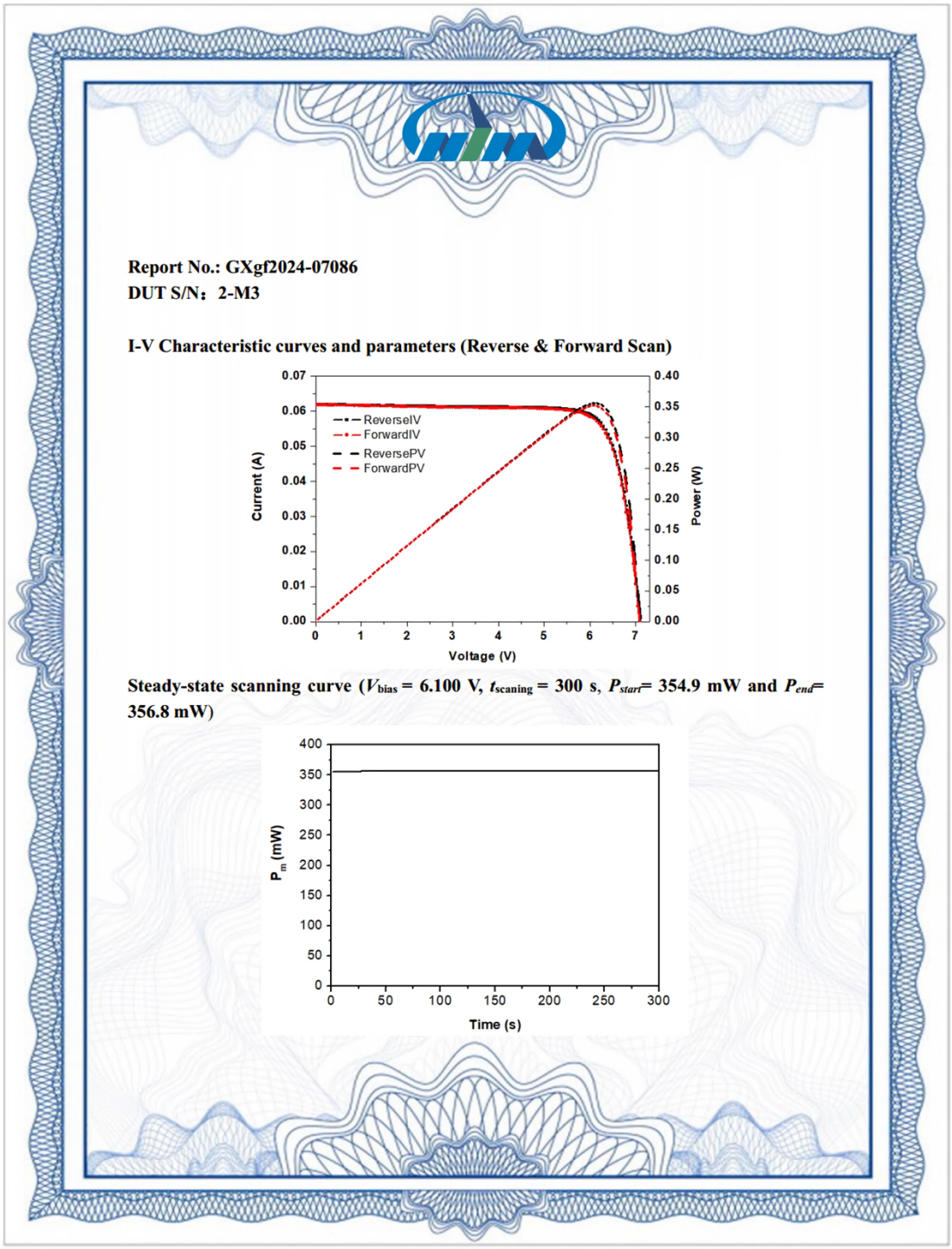

Supplementary Fig. 18 (Color online) Certified efficiency results of 14.6 cm^2 aperture area modules at an independent third-party photovoltaic laboratory (NIM, China).

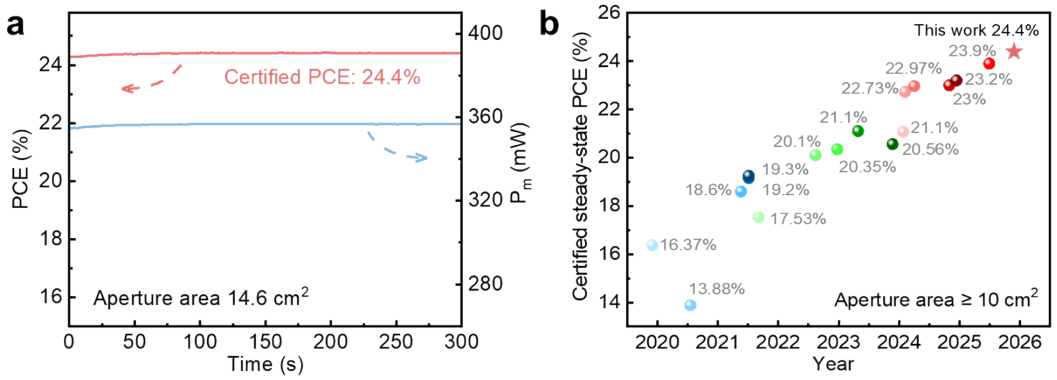

Supplementary Fig. 19 (Color online) (a) Certified steady-state power output of the 5 cm × 5 cm module (aperture area 14.6 cm^2), achieving a stable efficiency of 24.4%. (b) Certified steady-state PCE summary of reported perovskite photovoltaic modules (≥ 10 cm^2).

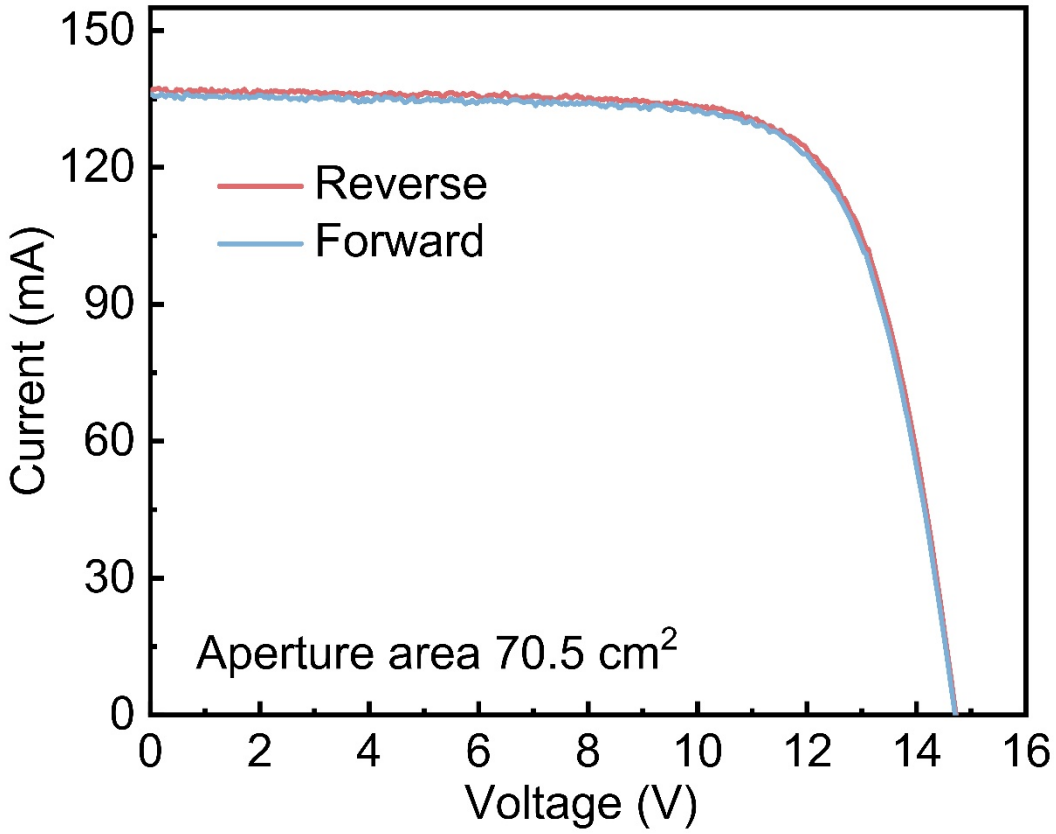

Supplementary Fig. 20 (Color online) *I-V* curves under forward and reverse scans of large-area perovskite module without NTG (70.5 cm^2 aperture area).

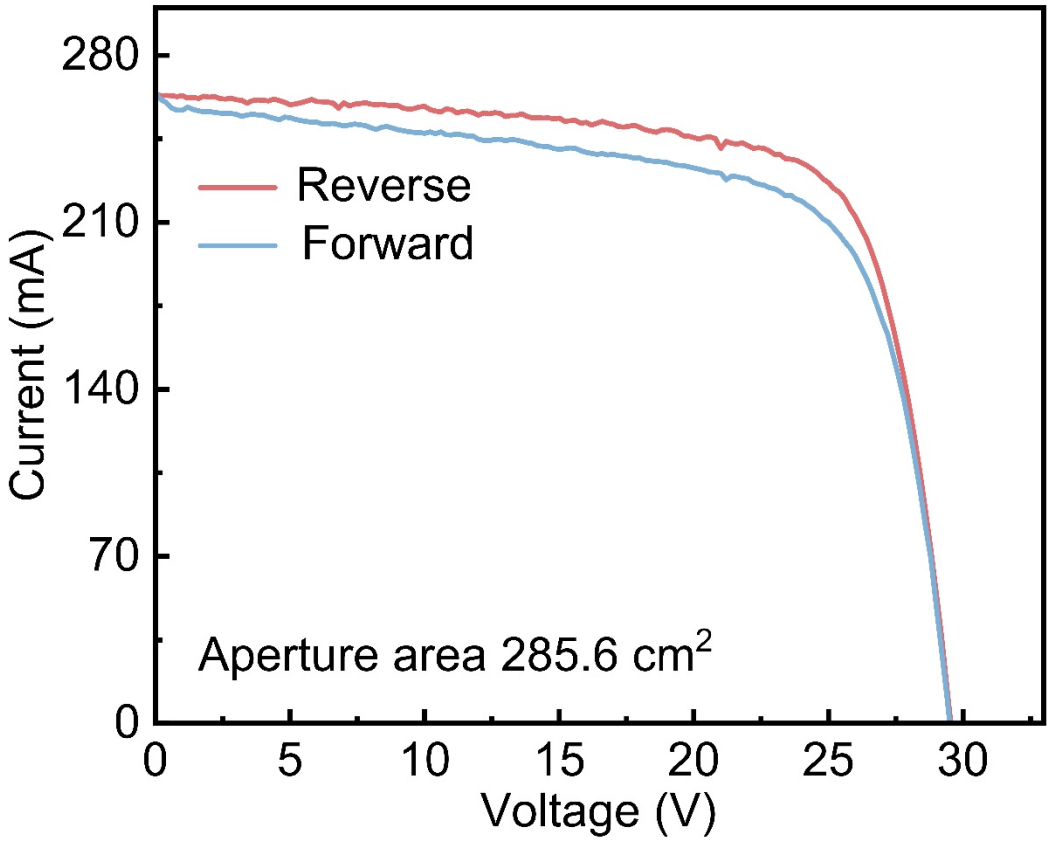

Supplementary Fig. 21 (Color online) *I-V* curves under forward and reverse scans of large-area perovskite module without NTG (285.6 cm^2 aperture area).

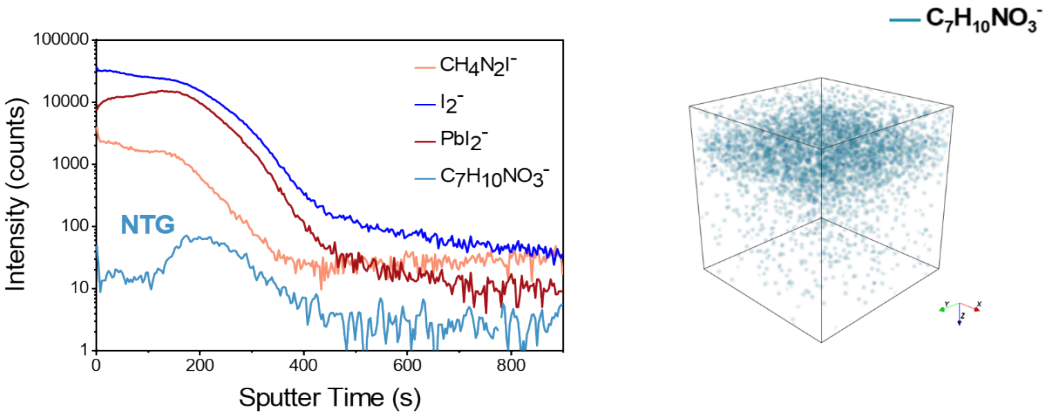

Supplementary Fig. 22 (Color online) The ToF-SIMS results of the target perovskite film with an architecture of Perovskite/Me-4PACz/NiO_x/FTO.

Supplementary Table 1 | Photovoltaic performance parameters of control and target perovskite solar cells with a 0.0725 cm^2 device area.

	V_{OC} (V)	J_{SC} (mA/cm^2)	FF (%)	PCE (%)
Reverse	1.19	26.57	85.3	26.99
Forword	1.19	26.55	84.9	26.83

Supplementary Table 2 | Photovoltaic performance parameters of control and target perovskite modules with a 14.6 cm^2 aperture area.

		V_{OC} (V)	I_{SC} (mA)	FF (%)	PCE (%)
Control	Reverse	6.828	61.3	79.36	22.74
	Forword	6.823	61.44	78.93	22.65
Target	Reverse	7.083	61.93	81.14	24.36
	Forword	7.095	61.7	80.95	24.26

Supplementary Table 3 | Photovoltaic performance parameters of control and target perovskite modules with a 70.5 cm^2 aperture area.

		V_{OC} (V)	I_{SC} (mA)	FF (%)	PCE (%)
Control	Reverse	14.73	136.8	74.02	21.2
	Forword	14.71	135.94	73.7	20.92
Target	Reverse	15.25	136.98	77.88	23.1
	Forword	15.18	136.9	77.29	22.8

Supplementary Table 4 | Photovoltaic performance parameters of control and target perovskite modules with a 285.6 cm^2 aperture area.

		V_{OC} (V)	I_{SC} (mA)	FF (%)	PCE (%)
Control	Reverse	29.54	263.72	72.8	19.9
	Forword	29.5	264.6	67.5	18.4
Target	Reverse	31.7	266.85	75.5	22.36
	Forword	31.55	267.4	74.1	21.89

Supplementary Table 5 | Aperture area, Concentration, Method, PCE, Structure, and Solvent of reported small-area and large area devices.

Area	Concentration	Method	Efficiency	Structure	Solvent	Ref.
~0.1 cm^2	1.8 M	Spin-coating	27.2% (certified)	pin	DMF/NMP	Science 390, 638-642 (2025).
	1.75 M		26.92% (certified)	pin	DMF/DMSO	Nature 646, 95–101 (2025).
	1.65 M		26.3% (certified)	pin	DMF/DMSO	Science 386, 898-902 (2024).
	1.67 M		26.15% (certified)	pin	DMF/DMSO	Science 384, 189-193 (2024).
	1.4 M		25.7% (certified)	nip	DMF/DMSO	Nature 616, 724–730 (2023).
	2 M		25.2% (certified)	pin	DMF/DMSO	Science 382, 1399-1404 (2023).
	1.6 M		25.1% (certified)	pin	DMF/DMSO	Science 382, 810-815 (2023).
	2.4 M		25.4% (certified)	nip	DMF/DMSO	Science 375, 302-306 (2022).
	1.73 M		24.3% (certified)	pin	DMF/DMSO	Science 376, 416-420 (2022).
	1.8 M		25.2% (certified)	nip	DMF/DMSO	Nature 592, 381–385 (2021).
11.7 cm^2	0.9 M	Blade-coating	22.69%	pin	DMF/NMP	Nat. Photon. 19, 968–976 (2025).
56.5 cm^2	1 M	Slot-die coating	21.5%	pin	DMF/DMPU	Nat Commun 16, 2052 (2025).
7200 cm^2	0.6 M	Slot-die coating	17.2% (certified)	pin	2MeTHF/GVL/DMSO	Science 390, 1021-1028 (2025).
20000 cm^2	1.2 M	Slot-die coating	20.05% (certified)	pin	DMF/NMP	Nature 648, 91–96 (2025).
27.22 cm^2	1.3 M	Spin-coating	23.3% (certified)	nip	DMF/DMSO	Nature 628, 299–305 (2024).
31 cm^2	1.3 M	Spin-coating	22.4%	nip	DMF/DMSO	Nat Energy 9, 316–323 (2024).
14.65 cm^2	1.3 M	Slot-die coating	22.96%	pin	DMF/NMP	Nat Commun 15, 6679 (2024).
26.9 cm^2	1.1 M	Blade-coating	21.8%	pin	2Me/DMSO	Science 380, 823-829 (2023).
27.83 cm^2	1.2 M	Spin-coating	21.4% (certified)	nip	DMF/DMSO	Nature 620, 323–327 (2023).

205 cm^2	1.25 M	Blade-coating	15.3%	nip	DMF/NMP	Nat Energy 7, 528–536 (2022).
174 cm^2	1.11 M	Slot-die coating	18.6%	pin	DMF/NMP	Joule 6, 1931-1943 (2022).
20.77 cm^2	1.3 M	Slot-die coating	17.2%	pin	DMF/NMP	Sci. Adv. 7, eabg3749 (2021).
31 cm^2	0.83 M	Bar-coating	20.4%	nip	2Me/CHP	Joule 5, 2420-2436 (2021).
29.5 cm^2	1.17 M	Blade-coating	18.6% (certified)	pin	ACN/2Me/DMSO	Nat Energy 6, 633–641 (2021).